ADVANCED MATERIALS

Supporting Information

for *Adv. Mater.*, DOI: 10.1002/adma.202001942

Pressure-Dependent Behavior of Defect-Modulated Band Structure in Boron Arsenide

Xianghai Meng, Akash Singh, Rinkle Juneja, Yanyao Zhang, Fei Tian, Zhifeng Ren, Abhishek K. Singh, Li Shi, Jung-Fu Lin, and Yaguo Wang**

Supporting Information

Pressure-Dependent Behavior of Defect-Modulated Band Structure in Boron Arsenide

Xianghai Meng†[1], Akash Singh†[2], Rinkle Juneja[2], Yanyao Zhang[3], Fei Tian[4], Zhifeng Ren[4], Abhishek K. Singh[3], Li Shi[1,5], Jung-Fu Lin[3,5], Yaguo Wang*[1,5]*

Section 1. Experimental Details

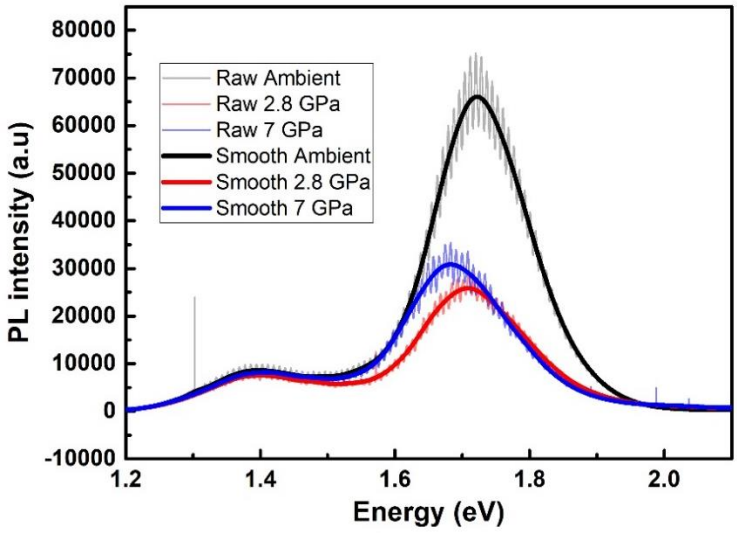

Figure S1. Examples of applying FFT filter to remove the oscillations causing by the interference from the front and bottom surfaces of BAs in PL measurement

Due to the transparent nature of the BAs crystal, the collected beams from the top and bottom surface of the crystal will interfere with each other and cause oscillations in the collected PL spectrum. We remove the oscillations by applying FFT filter. All the PL spectra presented in the main text are after removing the oscillations.

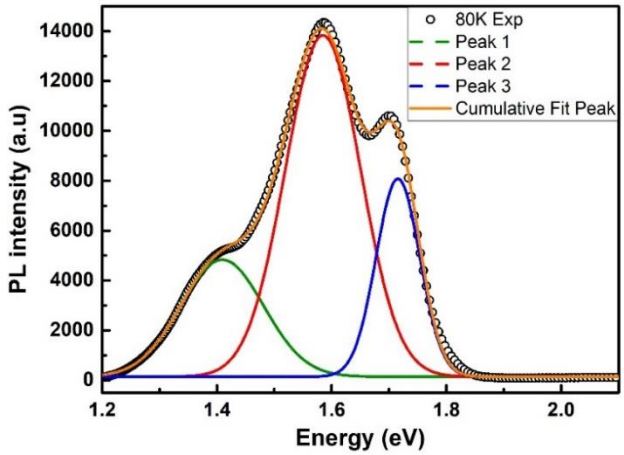

Figure S2. Example of three peak Gaussian fitting of the PL spectrum

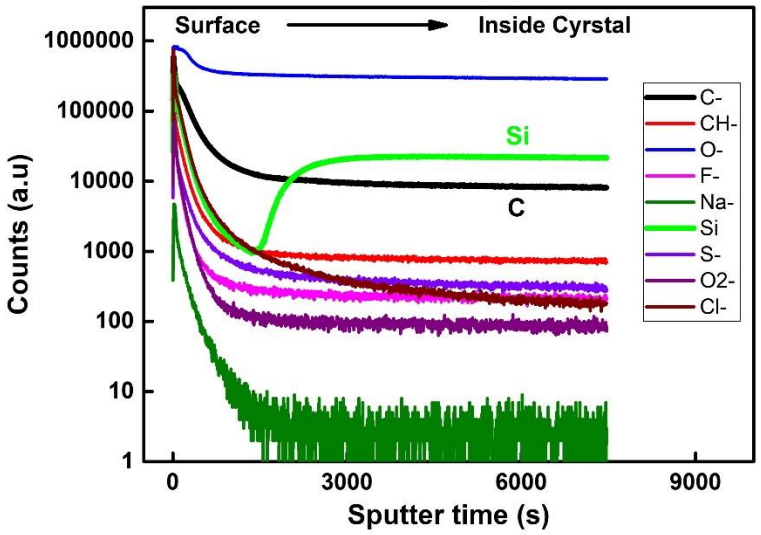

Figure S3. TOF-SMIS measurement showing the existence of Si and C impurities inside the BAs single crystal

Section 2. Simulation Details

All the structural relaxation and electronic structure calculations are performed using density functional theory (DFT) as implemented in the Vienna *ab initio* simulation package (VASP). As the defect property of any semiconductor are very sensitive to the band gap of that material and hybrid density functional approach, proposed by Heyd, Scuseria, and Ernzerhof (HSE06) provides an accurate description of the electronic structure and band gaps of semiconductors, therefore we have used HSE06 (25% exact exchange and 0.2 range separation) for the theoretical investigation of C and B impurities in cubic bulk BAs. The kinetic energy cutoff was set to 400

eV for the plane wave expansion. All the structures are completely relaxed until the Hellmann-Feynman forces is less than 0.005 eV/A˚. A Monkhorst-Pack k-point mesh of 13 × 13 × 13 is used for the relaxation of unit cell geometries as well as the convergence of charge density.
The defect [X] formation energy in charge state q is defined as

$$E_f[Xq] = E_{tot}^{defect} - E_{tot}^{pristine} - \sum n_i\mu_i + qE_F + \Delta^q \quad (1)$$

where E_{tot}^{defect} and $E_{tot}^{pristine}$ are the total energies of the defective and pristine supercells, respectively, n_i is the number of atoms of the i^{th} species, either added to ($n_i > 0$) or removed ($n_i < 0$) from the pristine supercell to form the isolated defect, μ_i is the chemical potential of the i^{th} element, E_F is the Fermi level with reference to valence band maxima (VBM), and Δ^q is the correction to the defect formation energy arising from the spurious interactions between charge images due to Periodic boundary condition (PBC).

The calculated optimized lattice parameter of cubic BAs is found to be a=4.81 Å, which is in good agreement in our experimental value of 4.79 Å. The hybrid DFT calculation (HSE06) gives an indirect band gap of 1.75 eV along the along the gamma-X path, which is in excellent agreement in our experimentally calculated value. In the first-principles methods, supercell approach is an ideal approach for the investigation defect properties. All the defect calculations have been performed for the 216 atoms contained supercell with 2 × 2 × 2 special K-points.
First, we did the first principle calculations of the possible native defects and found that all of them provide deep defect levels within the host band gap, and hence they cannot be the source of *p*-type conductivity in BAs. Therefore, intrinsic defects are not the source of unintentional *p*-type conductivity of BAs.

Having shown that intrinsic defect cannot be the source of *p*-type conductivity, we analyzed the defect thermodynamic of C and Si impurities, which we find in the c-BAs sample. To assess the stability of these impurities, we calculated the formation energies of the corresponding defects. The defect thermodynamics predicts that the concentration of Si based impurities (i.e. Si_{As} and Si_B) is higher than the C based impurities (i.e. C_{As} and C_B), as the formation energies of Si impurities are low compared the C impurities. Interestingly, we find that these impurities are always ionized i.e. either +1 or -1, for the wide range of Fermi-level. These impurities are most stable in their positive charge state, i.e. +1, when the Fermi level approaches the valence band

maxima (VBM) (i.e. *p*-type condition) and become most stable in -1 charge state, when Fermi-level approaches towards the conduction band minima (CBM) (i.e. *n*-type condition). Therefore, these impurities compensating their corresponding electrical conductivity.

The (0/-1) level of Si_{As} occurs at 0.06 eV above the VBM, which is almost in resonant with VB and hence is a shallow acceptor defect. The ionization energy of Si_{As} is in the range of few k_BT, therefore Si impurities lead the *p*-type conductivity in BAs. C_{As} is a donor defect and the (+1/0) level occurs 0.14 eV below the CBM, which is a deep donor level and cannot lead *n*-type conductivity. The slopes of Si_{As}^{-1} and C_{As}^{+1} cross to each other near valence band and force to the Fermi level to lies at the crossing point, which is known as pinned Fermi-level. The pinned Fermi level locates at E_F^{Pinned}= E_{VBM} + 0.18 eV. The (0/-1) level of C_{As} locate at 0.08 eV above the VBM, which make it a shallow acceptor defect. C_B is found to be a deep donor defect and the (+1/0) level occurs 0.29 eV below the CBM. C impurities pine the Fermi levels towards the middle of the band gap and locate at E_F^{Pinned} = E_{VBM} + 0.43 eV. Therefore, our defect thermodynamic analysis of C and As impurities predict that the Fermi level locate between 0.2 eV to 0.4 eV above the VBM, in the thermodynamic equilibrium position. Hence, this pinned Fermi level, which is close to VBM, indicates the *p*-type conductivity of c-BAs.

The static dielectric tensor of BAs was calculated using the density functional perturbation theory (DFPT) implemented with the projector-augmented wave method in the Vienna ab initio simulation package (VASP).[1, 2] Electronic exchange and correlation was approximated by the Perdew-Burke-Ernzerhof (PBE) form of the generalized gradient approximation (GGA). All the structures are completely relaxed until the Hellmann-Feynman forces is less than 0.005 eV/A^0. A Monkhorst-Pack k-point mesh of 13 × 13 × 13 is used for the relaxation of unit cell geometries as well as the convergence of charge density. The electronic wave functions are expanded in plane waves with energy up to 400 eV.

Optical properties are calculated within the GW-BSE formalism as implemented in the BERKELEYGW package.[3] The dielectric matrix is calculated within the random phase approximation (RPA) and expressed in a plane-wave basis with plane-wave energies up to 400

eV. In the case of unit cell calculations, we include 500 bands while performing the sum over unoccupied states involved in the dielectric matrix and self-energy calculations. To ensure the convergence of our results with the number of bands, we added a static remainder term to the self-energy.[4]

Section 3. Formation Energy of O_B and O_{As} in BAs

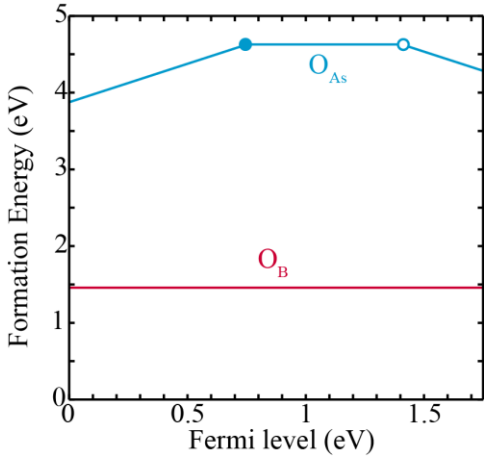

Figure S4. Simulation of formation energy of O_B and O_{As} in BAs

Donor-acceptor-pair (DAP) is created between donors and acceptors, which means the elements should be able to form both donor and acceptor levels in BAs. Since boron and arsenic have 3 and 5 valence electrons, respectively, only elements with 4 valence electrons on the outer shell, such as Si and C, can occupy both the B and As site, to form DAP. Other elements may not be able to form DAP. Secondly, to form DAP at both donor and acceptor levels, the defect state should not be too deep or too close to the middle of the bandgap. With deep donor/acceptor levels, the ionization energy could be so large that the defects cannot be activated initially to form DAP pairs. From our simulation of oxygen formation energy, as shown in **Figure S4**, O_B is always stable as neutral charge state, meaning O_B will not provide any donor acceptor pair recombination. On the other hand, O_{As} provides very deep donor and acceptor levels with high formation energy, which is also unlikely to form DAP. Thus, we can conclude that it is not possible to observe O-related DAP peaks in our PL measurements.

Section 4. Macroscopic Static Dielectric Tensor of BAs at Different Pressures

Table S1. Macroscopic static dielectric tensor of BAs with pressure. Z* is Born effective charge.

Pressure (GPa)	Dielectric tensor	Z*(B)
0	$\varepsilon_{xx}= \varepsilon_{yy}= \varepsilon_{zz}$ = 9.83	-0.46
4.5	$\varepsilon_{xx}= \varepsilon_{yy}= \varepsilon_{zz}$ = 9.62	-0.63
8.8	$\varepsilon_{xx}= \varepsilon_{yy}= \varepsilon_{zz}$ = 9.43	-0.82
14.3	$\varepsilon_{xx}= \varepsilon_{yy}= \varepsilon_{zz}$ = 9.29	-1.00
20	$\varepsilon_{xx}= \varepsilon_{yy}= \varepsilon_{zz}$ = 9.18	-1.19

Section 5. Comparison of simulation results with HSE06 and other methods (GW, LDA, etc)

What summarized in Table S2 are the simulations of the bandgap of BAs with DFT and beyond. In general, LDA underestimates the bandgap, with values around 1.2 eV (Ref 2[5] & 8[6]). With GW method, early results (Ref 5 in 1991[7]) predicted a bandgap around 1.6 eV. Recent GW results (Ref 1 in 2020[8] and Ref 2 in 2019[5]) predicted an indirect bandgap larger than 2.0 eV. We have also performed a simulation with GW, which gives a quasiparticle bandgap about 2.12 eV, consistent with the recent GW results (**Figure S5**). Usually the quasiparticle bandgap predicted with GW is higher than the optical bandgap, latter of which is measured in this work. With HSE06 method, most of the results in literature lie between 1.6 eV and 1.9 eV, consistent with our experimental and simulation results.

Even though HSE06 also predicts a quasiparticle bandgap, it is the most popular approach to simulate the optical and thermodynamic transitions associated with defect levels,[9-12] while GW method is seldom used for this purpose. In order to calculate the optical bandgap very accurately, we need to perform computationally expensive BSE calculations, which is currently beyond our computational resources.

By considering all these factors mentioned above, it is reasonable to compare our measured optical bandgap with simulations by HSE06.

Table S2. Simulated indirect bandgap of BAs with different methods

	Ref	Indirect (eV)	method
1	Song, B. et al. Optical properties of cubic boron arsenide. Appl. Phys. Lett. 116, 141903 (2020).	2.07	GW (quasiparticle bandgap)
2	Bushick, K., Mengle, K., Sanders, N. & Kioupakis, E. Band structure and carrier effective masses of boron arsenide: Effects of quasiparticle and spin-orbit coupling corrections. Appl. Phys. Lett. 114, 022101 (2019).	1.19	LDA (quasiparticle corrections)
		2.115	GW
3	Ge, Y., Wan, W., Guo, X. & Liu, Y. Direct and indirect optical absorptions of cubic BAs and BSb. Opt. Express 28, 238-248 (2020).	1.84	HSE
4	Zheng, Q. et al. Antisite pairs suppress the thermal conductivity of BAs. Phys. Rev. Lett. 121, 105901 (2018).	1.2	PBE
		1.62	HSE
5	Surh, M. P., Louie, S. G. & Cohen, M. L. Quasiparticle energies for cubic BN, BP, and BAs. Phys. Rev. B 43, 9126 (1991).	1.6	GW
6	Buckeridge, J. & Scanlon, D. O. Electronic band structure and optical properties of boron arsenide. *Physical Review Materials* **3**, 051601 (2019).	1.674	GW
7	Chae, S., Mengle, K., Heron, J. T. & Kioupakis, E. Point defects and dopants of boron arsenide from first-principles calculations: Donor compensation and doping asymmetry. *Appl. Phys. Lett.* **113**, 212101 (2018).	1.9	HSE

8	Chimot, N., Even, J., Folliot, H. & Loualiche, S. Structural and electronic properties of BAs and BxGa1− xAs, BxIn1− xAs alloys. Physica B: Condensed Matter 364, 263-272 (2005).	1.1	LDA
		1.87	LDA + GW
9	Ahmed, R., Hashemifar, S. J., Akbarzadeh, H. & Ahmed, M. Ab initio study of structural and electronic properties of III-arsenide binary compounds. Comput. Mater. Sci. 39, 580-586 (2007).	1.13	LDA
		1.18	GGA
		1.79	GGA-EV

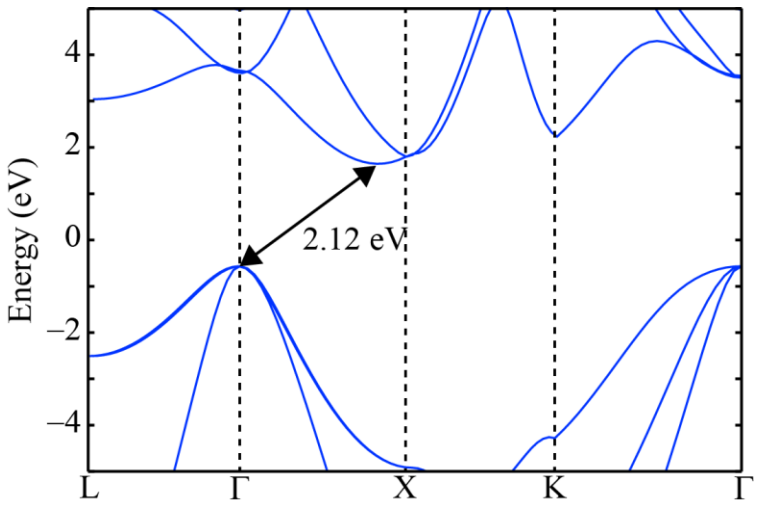

Figure S5. Simulated GW bandgap

Section 6: Temperature dependent optical bandgap of BAs

The indirect optical bandgap of BAs shows a weak dependence on the temperature. Firstly, it is necessary to clarify the origin of the temperature-dependent bandgap in semiconductor. At lower temperature, the interatomic spacing decreases and also the thermal energy of the carriers. The decrease in interatomic spacing causes the increase of the lattice potential seen by the electrons in the material, which increases the bandgap. So the thermal expansion coefficient is a parameter

that's positively correlated with the temperature dependent bandgap. As seen in **Figure S6**, for materials (GaAs, Ge) with large thermal expansion coefficients, their bandgaps are more sensitive to temperature. For silicon and diamond, with a relatively small thermal expansion coefficient, their bandgaps are much less sensitive to temperature change. Since BAs have a relatively small thermal expansion coefficient of $3.85*10^{-6}$ K^{-1},[13] its bandgap would increase with decreasing temperature, but the change should be small.

Secondly, when the temperature decreases, thermal energy of carriers decreases, resulting more localized electron/holes on the donor/acceptor levels. By looking at our peak intensity vs. temperature, this effect is significant. According to previous studies, free-carrier screening can result in blueshift of optical transition (larger bandgap).[14-16] In our measurement, the lower temperature suppresses the free-carriers in BAs, which have an opposite effect, meaning smaller bandgap.

Thirdly, the phonon-assisted indirect bandgap transition is minimal due to the fact that thermal energy is only on the order of meV, which could not contribute to significant change of the optical transition at different temperatures. Considering all the factors mentioned above, when lowering the temperature, the small increase trend in bandgap from the shrinkage of interatomic spacing will be offset by the weakened free-carrier screening effect, thus the bandgap variation with temperature is small.

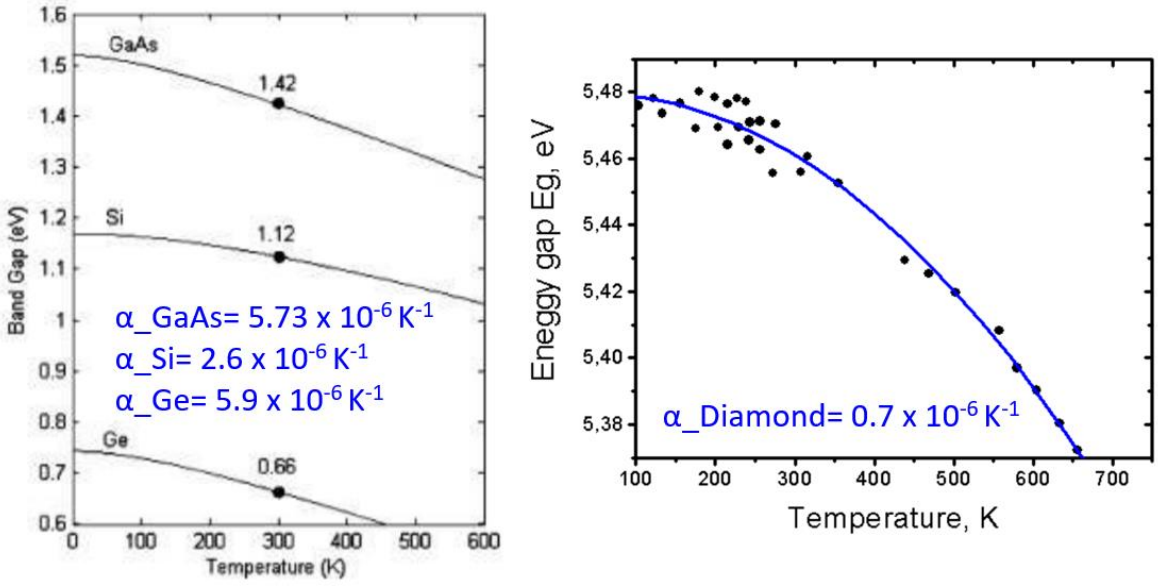

Figure S6. Bandgap vs. temperature of different semiconductors and diamond[17, 18]

Section 7: Cconcentration of C Impurities

The concentration of C_B and C_{As} are simulated at the sample growth temperature (~1200 K). Results in literature report that BAs is p-doped,[19, 20] and the Fermi level should lie closer to valence band maximum (VBM) than to conduction band minimum (CBM), so we choose the concentration of C_B and C_{As} at VBM, which is an extreme case. At VBM, the concentration of C_B is 1.53 x 10^{14} cm^{-3}, and of C_{As} is 6.36 x 10^{10} cm^{-3}. In the literature, usually the concentration of DAP defects that induces photoluminescence falls into the range of 10^{15} to 10^{18} cm^{-3}.[21-23] Comparing with those values, the C_B/C_{As} concentrations estimated in our sample at VBM are not negligible. Also we need to keep in mind that the reference for the formation energy of C used in our simulation is graphite, which gives the upper limit of formation energy. With reference C in other forms, the formation energy could be much lower, which will lead to even higher C_B/C_{As} concentration, since the concentration will increase exponentially with decreasing formation energy. The C impurity has been predicted to exist in BAs by other simulation works as well.[19, 24]

With Fermi level at VBM, which is an extreme case, the C_B concentration is about 1000 times of that of C_{As}. In reality, for p-doped semiconductors (not heavily doped), the Fermi level is not at the VBM but should be higher than that (still closer to VBM compared to CBM). This applies to be the case in our sample, since we did not purposely dope the sample. Then the difference in concentrations of C_B and C_{As} should not be this large. For example, if the Fermi level is at ~ 0.5 eV above VBM, the formation energy of C_B and C_{As} would be similar (Figure1 in the maintext), and the concentration of C_B and C_{As} would be comparable. In addition, the PL peak intensity does not only depend on the concentration, it also depends on the quantum efficiency (QE). If C-DAP has a much higher QE than Si-DAP, even with much smaller concentration C may result in comparable PL intensity with Si-DAP.

In summary there are non-negligible amount of C impurities in our BAs crystal and their contribution to the DAP levels is significant.

Section 8: Vertical (optical) transitions of e/h to the relevant band edge

The DAP peak is realated to the vertical transition levels and the information of these transition can be obtained through the defect Kohn-Sham levels. Our results suggest that Si_{As} provides shallow acceptor level near the valence band and Si_B provides shallow donor level near the

conduction band. The wave function associated with these defect Kohn-Sham levels are delocalized over several lattice sites, which results ionization of these defects, easily.

The acceptor levels by Si_{As} and donor levels by Si_B, are located at 0.11 eV below the conduction band minima and 0.08 eV above to the valence band maxima, respectively. The schematic of these levels are shown in Figure S7. The emitted photon energy for an infinitely distant donor-acceptor pair $E_\infty = E_g - (E_d + E_a) = 1.56$ eV, which is in well agreement with our experimental value i.e., 1.5 eV. The observed PL emission band has been attributed to the radiative recombination of an electron occupying a donor level ($E_d = 0.11$ eV) and a hole occupying an acceptor level ($E_a = 0.08$ eV).

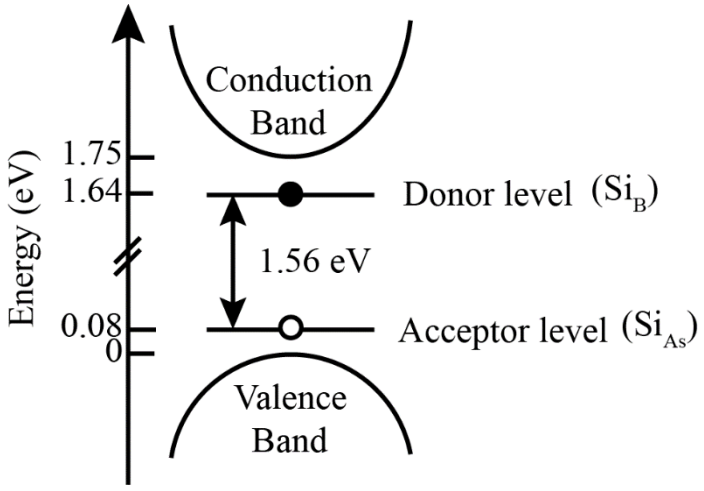

Figure S7. Proposed energy level diagram of DAP recombination by Si impurities in BAs.

Section 9: Simulations of pressure-dependent bandgap with GW method

The change of band structure with pressure were simulated and presented in **Figure S8**. At the ambient pressure the position of VBM occurs at the Γ point, while the conduction band minimum (CBM) is found along the Γ to X direction at k-point with crystal coordinates (0.39, 0.00, 0.39), about 80% of the distance to the X point. The previous report,[5] suggests that the VBM is made up of 57.6% boron p-orbitals and 40.2% arsenic p-orbitals. The CBM is made up of 30.9% boron p-orbitals, 24.0% boron s-orbitals, 20.1% arsenic p-orbitals, and 15.4% arsenic s-orbitals. The calculated smallest direct gap occurs at the Γ point with a value of 3.95 eV.

As the pressure increases, the CBM shifts downward and closer to X point and VBM shifts upward but fixed Γ point. The combined effect of this shift results in decrease of the indirect band gap from 1.75 eV to 1.54 eV as a function of pressure. This decrease of indirect band gap as a function of pressure is consistent with the experimental PL spectra, as shown in Figure 3b in the main manuscript. On the other hand, the calculated direct band gap of 3.95 eV at Γ point increases with pressure. Furthermore, the transitions at other high symmetry points such as L-L, K-K, X-X all show an increasing trend with pressure. In summary, the direct band gap and transitions at all high symmetry points increase with pressure, while the indirect bandgap in our measurement is the only transition that decreases with pressure.

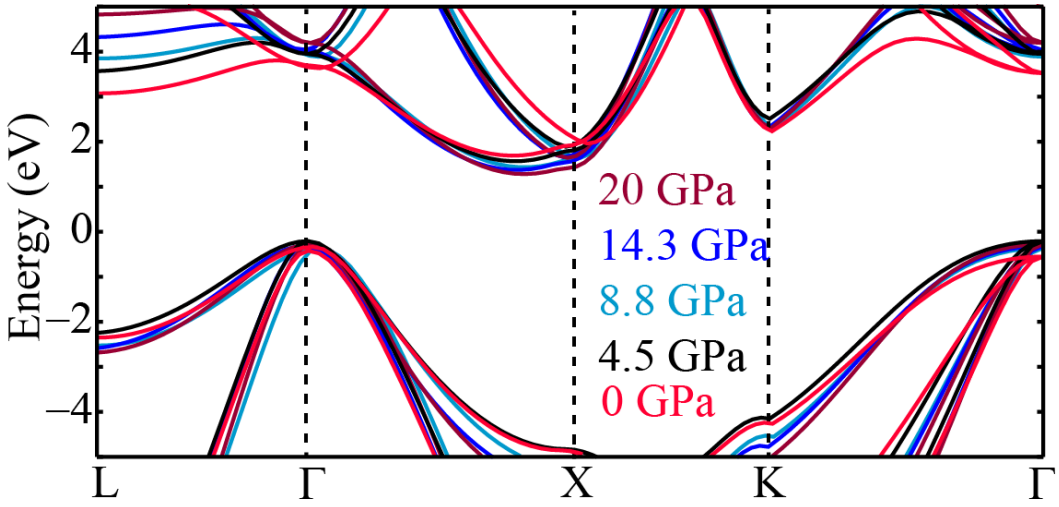

Figure S8. Pressure dependent electronic band structure of BAs

Figure S9 shows the absolute band alignment of BAs relative to the vacuum level as a function of pressure. The band gap is always reduced systematically as the pressure increases. The position of VBM shifts upward, and the position of CBM shifts downward. At 20 GPa, the indirect band gap is reduced by 12%.

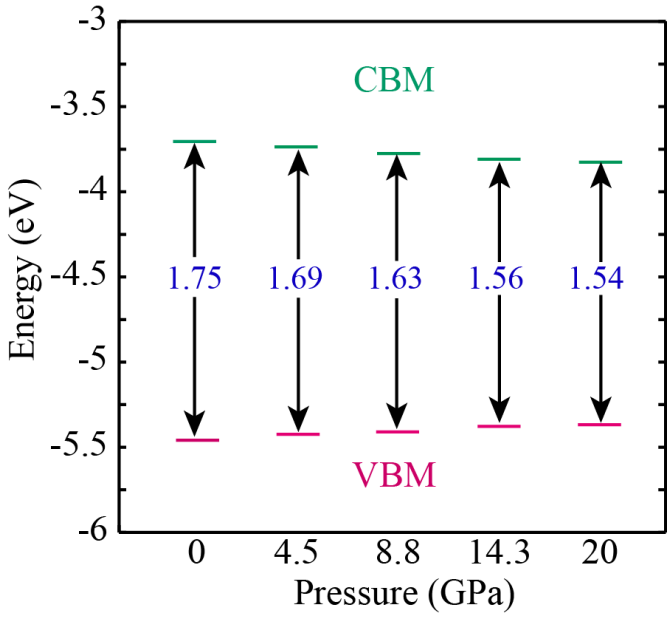

Figure S9. Absolute band alignments of BAs relative to the vacuum level with pressure.

Figure S10 shows the effects of compressive and tensile strain on the absolute band positions. We examine the effects of strain on the band structure along x direction (***a*** axis), at both the conduction band minimum (CBM) and valence band maximum (VBM). The absolute band positions are quite sensitive to strain. Both compressive and tensile strain uplifts the VBM and downshifts the CBM. With 3.8% compressive strain, the indirect bandgap decreases from 1.75 eV to 1.54 eV; with 3.8% compressive strain, the indirect bandgap decreases from 1.75 eV to 1.48 eV.

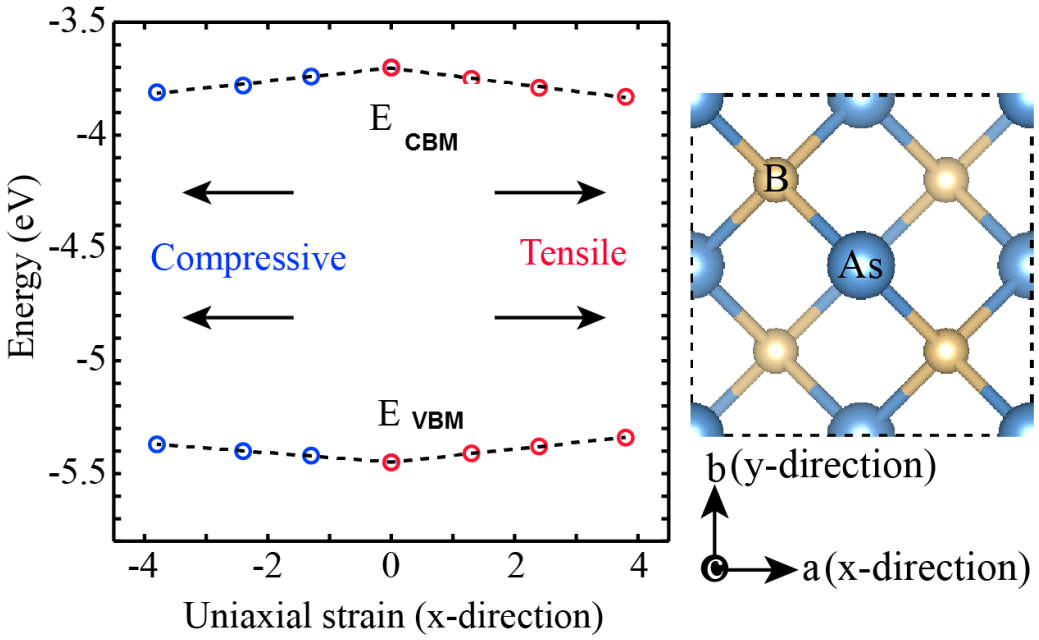

Figure S10. Variation in E_{VBM} and E_{CBM} at absolute band position with the function of uniaxial strain along x direction.

The deformation potential can be estimated from the slope of these straight lines in **Figure S10**. The variation of the band edge position with respect to strain is linear. Under the compressive strain, the variation of E_{VBM} and E_{CBM} follow: y = -0.021x -5.45 and y = 0.029x -3.70, respectively. Under the tensile strain, the variation of E_{VBM} and E_{CBM} follow: y = -0.028x -5.45 and y = 0.034x -3.70, respectively. Therefore, the deformation potential at Γ point is nearly 0.02 eV and at Γ-X direction is about 0.03 eV. Larger deformation potential of CBM indicates the conduction bands are more sensitive to the applied uniaxial strain as compared to valence bands, and hence are mainly responsible for decrease in the band gap.

Reference

[1] A. Debernardi, S. Baroni, Solid State Commun. 1994, 91, 813.
[2] A. Singh, A. Manjanath, A. K. Singh, J. Phys. Chem. C 2018, 122, 24475.
[3] J. Deslippe, G. Samsonidze, D. A. Strubbe, M. Jain, M. L. Cohen, S. G. Louie, Comput. Phys. Commun. 2012, 183, 1269.
[4] J. Deslippe, G. Samsonidze, M. Jain, M. L. Cohen, S. G. Louie, Phys. Rev. B 2013, 87, 165124.
[5] K. Bushick, K. Mengle, N. Sanders, E. Kioupakis, Appl. Phys. Lett. 2019, 114, 022101.
[6] N. Chimot, J. Even, H. Folliot, S. Loualiche, Physica B: Condensed Matter 2005, 364, 263.
[7] M. P. Surh, S. G. Louie, M. L. Cohen, Phys. Rev. B 1991, 43, 9126.

[8] B. Song, K. Chen, K. Bushick, K. A. Mengle, F. Tian, G. A. G. U. Gamage, Z. Ren, E. Kioupakis, G. Chen, Appl. Phys. Lett. 2020, 116, 141903.
[9] C. Freysoldt, B. Grabowski, T. Hickel, J. Neugebauer, G. Kresse, A. Janotti, C. G. Van de Walle, Rev. Mod. Phys. 2014, 86, 253.
[10] A. Alkauskas, P. Broqvist, A. Pasquarello, Phys. Rev. Lett. 2008, 101, 046405.
[11] A. Singh, A. K. Singh, Phys. Rev. B 2019, 99, 121201.
[12] Y. Frodason, K. Johansen, T. Bjørheim, B. Svensson, A. Alkauskas, Phys. Rev. B 2017, 95, 094105.
[13] J. S. Kang, M. Li, H. Wu, H. Nguyen, Y. Hu, Appl. Phys. Lett. 2019, 115, 122103.
[14] D. Reynolds, D. C. Look, B. Jogai, J. Appl. Phys. 2000, 88, 5760.
[15] S. Chun, J. Appl. Phys. 1996, 80, 4773.
[16] H. Schweizer, A. Forchel, A. Hangleiter, S. Schmitt-Rink, J. Löwenau, H. Haug, Phys. Rev. Lett. 1983, 51, 698.
[17] L. N. Nascimento, L. C. L. A. Jamshidi, C. M. B. de Menezes Barbosa, R. J. Rodbari, Revista Tecnológica 2015, 24, 81.
[18] C. Clark, P. Dean, P. Harris, Proceedings of the Royal Society of London. Series A. Mathematical and Physical Sciences 1964, 277, 312.
[19] J. L. Lyons, J. B. Varley, E. R. Glaser, J. A. Freitas Jr, J. C. Culbertson, F. Tian, G. A. Gamage, H. Sun, H. Ziyaee, Z. Ren, Appl. Phys. Lett. 2018, 113, 251902.
[20] S. Wang, S. F. Swingle, H. Ye, F.-R. F. Fan, A. H. Cowley, A. J. Bard, J. Am. Chem. Soc. 2012, 134, 11056.
[21] A. Liu, H. T. Nguyen, D. Macdonald, IEEE Journal of Photovoltaics 2017, 7, 581.
[22] D. Toginho Filho, I. Dias, J. Duarte, E. Laureto, J. C. Harmand, BrJPh 2005, 35, 999.
[23] M. Tajima, T. Iwai, H. Toyota, S. Binetti, D. Macdonald, J. Appl. Phys. 2011, 110, 043506.
[24] S. Chae, K. Mengle, J. T. Heron, E. Kioupakis, Appl. Phys. Lett. 2018, 113, 212101.